RESEARCH ARTICLE

EFA6A, an exchange factor for Arf6, regulates early steps in ciliogenesis

Mariagrazia Partisani[1], Carole L. Baron[1], Rania Ghossoub[2], Racha Fayad[1], Sophie Pagnotta[3], Sophie Abélanet[1], Eric Macia[1], Frédéric Brau[1], Sandra Lacas-Gervais[3], Alexandre Benmerah[4], Frédéric Luton[1] and Michel Franco[1],*

ABSTRACT

Ciliogenesis is a coordinated process initiated by the recruitment and fusion of pre-ciliary vesicles at the distal appendages of the mother centriole through mechanisms that remain unclear. Here, we report that EFA6A (also known as PSD), an exchange factor for the small G protein Arf6, is involved in early stage of ciliogenesis by promoting the fusion of distal appendage vesicles forming the ciliary vesicle. EFA6A is present in the vicinity of the mother centriole before primary cilium assembly and prior to the arrival of Arl13B-containing vesicles. During ciliogenesis, EFA6A initially accumulates at the mother centriole and later colocalizes with Arl13B along the ciliary membrane. EFA6A depletion leads to the inhibition of ciliogenesis, the absence of centrosomal Rab8-positive structures and the accumulation of Arl13B-positive vesicles around the distal appendages. Our results uncover a novel fusion machinery, comprising EFA6A, Arf6 and Arl13B, that controls the coordinated fusion of ciliary vesicles docked at the distal appendages of the mother centriole.

KEY WORDS: Arf6, Rab8, Arl13B, DAVs fusion, EFA6A, Ciliogenesis, Membrane trafficking

INTRODUCTION

The primary cilium (PC) is a microtubule-based structure found in most eukaryotic cells. Originally considered to be a vestigial organelle, it is now the object of intense interest because of its essential roles in cell homeostasis and development. In addition, defects in PC assembly or function cause a wide variety of diseases called ciliopathies. They include skeletal defects, limb and digit development disorders, cystic renal diseases, neurodevelopmental disorders (cerebellar hypoplasia and/or ataxia, acrocallosal syndrome) and retinal degeneration (Badano et al., 2006; Hildebrandt et al., 2011; Thomas et al., 2019; Tobin and Beales, 2009). Considered as a group, the prevalence rate of ciliopathies is relatively high (1 in 2000 adults) (Quinlan et al., 2008). These disorders are due to mutations in genes that encode proteins localized to the PC and which play an important role in its assembly and/or function.

The PC is formed at the distal end of the mother centriole (m-centriole) during quiescence or the G0 phase of the cell cycle (Ishikawa and Marshall, 2011; Malicki and Johnson, 2017; Sanchez and Dynlacht, 2016). The assembly of PC starts with the formation of a large ciliary vesicle (CV) docked to the m-centriole as described a long time ago by Sergei Sorokin (Sorokin, 1962). This step is followed by the dissociation of the inhibitory CP110–CEP97 complex (CP110 is also known as CCP110) from the distal end of the m-centriole allowing extension of the axoneme within the CV and the formation of the cilium (reviewed in Ishikawa and Marshall, 2011; Sanchez and Dynlacht, 2016). However, the biogenesis of the CV is not fully understood. Recent reports describe the presence of small pre-ciliary vesicles docked onto the distal appendages of the m-centriole (also called DAVs, for distal appendage vesicles) that precede the formation of the CV, through their fusion (Lu et al., 2015b; Wu et al., 2018). The DAV fusion is driven by the proteins EHD1 and/or EHD3 and the SNARE SNAP29, at the very least (Lu et al., 2015b). Then, the extension of the CV and the ciliary membrane biogenesis is achieved by vesicular membrane trafficking controlled by a cascade of small G proteins, including Rab11 and Rab8 (herein referring collectively to the Rab8a and Rab8b, and Rab11a and Rab11b forms) (Knodler et al., 2010; Nachury et al., 2007; Westlake et al., 2011). More precisely, continuous fusion of Rab8-positive structures is responsible for the PC membrane formation (Sanchez and Dynlacht, 2016). The Rab8 guanine nucleotide exchange factor (GEF) Rabin8 (also known as RAB3IP) is activated and recruited by Rab11-containing recycling endosomes (Blacque et al., 2005; Sanchez and Dynlacht, 2016). In accordance with their crucial role in PC formation, it has been observed that depletion of Rabin8 or overexpression of a dominant-negative mutant of Rab8 abolishes ciliogenesis, whereas overexpression of a constitutively activated Rab8 leads to ciliary membrane extension (Nachury et al., 2007; Yoshimura et al., 2007). More recently, the exocyst, an octameric protein complex implicated in the tethering and fusion of post-Golgi and recycling-compartment-derived vesicles with the plasma membrane, has also been shown to control ciliogenesis and ciliary membrane extension (Lobo et al., 2017; Zuo et al., 2009). Indeed, the exocyst complex localizes to the PC, and knockdown of Sec10 (also known as EXOC5), one of the eight exocyst subunits, strongly inhibits ciliogenesis, whereas its overexpression increases PC assembly and length (Rogers et al., 2004; Zuo et al., 2009). Moreover, Sec15 (also known as EXOC6), another exocyst subunit, interacts with Rab proteins including Rab8 and Rab11 (reviewed in Das and Guo, 2011). Arl13B is another small G protein that is involved in membrane transport, and a set of mutations in the corresponding gene has been linked to the Joubert syndrome ciliopathy, indicating that it plays a key role in ciliary

functions (Barral et al., 2012; Cantagrel et al., 2008; Sun et al., 2004). Arl13B regulates the ciliary length by controlling ciliary membrane extension (Lu et al., 2015a). In addition, Arl13B acts as an Arl3 GEF to control the ciliary targeting of lipidated protein cargo, and the assembly of intraflagellar transport (IFT)-A and -B complexes, which are required for the intra-cilium transport (Gotthardt et al., 2015; Ivanova et al., 2017). Interestingly, Arl13B also directly binds two exocyst complex subunits, Sec5 and Sec8 (EXOC2 and EXOC4, respectively), indicating that Arl13B and the exocyst might function together to control ciliary membrane extension via the tethering of membrane vesicles (Seixas et al., 2016).

The EFA6 family belongs to the Sec7-domain-containing protein family that act as GEFs for the small G protein Arf6, a member of the ADP-ribosylation factor (Arf) group (Franco et al., 1999). Humans express four tissue specific EFA6 isoforms, which are encoded by four different genes (D'Souza-Schorey and Chavrier, 2006; Sakagami, 2008). While they display highly divergent N-terminal domains, they share a common C-terminal structure (Derrien et al., 2002). Despite their homology and frequent co-expression, it remains unclear whether the different EFA6 proteins play specific or overlapping roles. EFA6A (also known as PSD), is mostly expressed in the brain, small intestine and colon (Derrien et al., 2002). It controls the endocytic trafficking of different cargoes, such as GPCRs, the transferrin receptor and ion channels (Decressac et al., 2004; Franco et al., 1999; Gong et al., 2007; Macia et al., 2012), and the transport of membrane vesicles to form the apical lumen in mammary epithelial cells (Zangari et al., 2014). In addition, EFA6A drives actin cytoskeleton reorganization, at least in part, by interacting with F-actin and α-actinin (Macia et al., 2008; Macia et al., 2019; Milanini et al., 2018; Sakagami et al., 2007). Its exogenous expression leads to the formation of membrane ruffles in various cell types, the stabilization of the apical actomyosin ring in polarized epithelial cells (Derrien et al., 2002; Franco et al., 1999; Luton et al., 2004), the formation of neurite and dendritic spines (Choi et al., 2006; Sakagami et al., 2007; Sironi et al., 2009) and axon regeneration (Eva et al., 2017).

Arf6, the substrate of EFA6, is also involved in vesicular transport. It regulates the internalization of certain cargoes in a mechanism which remains to be established. In addition, Arf6 controls the recycling of proteins from endosomal structures back to the plasma membrane (D'Souza-Schorey and Chavrier, 2006). A compilation of numerous studies gives an overview of the molecular mechanism involving Arf6 in the recycling pathway. Indeed, via its direct interaction with the AP-2 complex, Arf6 leaves the plasma membrane with AP-2- and clathrin-coated vesicles (Donaldson and Jackson, 2011). Once associated with endosomal membranes, Arf6 binds to a microtubule motor adaptor (JIP3 and JIP4) to allow for the recycling of vesicles (Montagnac et al., 2009). By interacting with the Sec10 subunit of the exocyst complex, Arf6 regulates the delivery of and insertion of recycling membranes to regions of the plasma membrane (Prigent et al., 2003). Arf6 has also been linked to Arl13B in the endocytic recycling pathway of certain membrane receptors. Both proteins colocalize onto endocytic intracellular structures and recycling vesicles enriched in clathrin independent cargoes (Barral et al., 2012). Interestingly, Arf6 has also been linked to Rab8 and EHD1 and, hence, the regulation of trafficking of non-clathrin cargoes. Arf6, Rab8 and EHD1 colocalize and functionally interact on cytoplasmic tubular compartments during the recycling of cargoes internalized by clathrin-independent endocytosis (Caplan et al., 2002; Hattula et al., 2006). It has been shown that the formation and the function of these tubular organelles are strictly dependent on the activity of the two small G proteins Rab8 and Arf6 (Hokanson and Bretscher, 2012; Peranen, 2011).

The fact that EFA6A and Arf6 are involved in the establishment of epithelial cell polarity and the vesicular membrane trafficking in partnership with proteins known to be involved in ciliogenesis (Rab8, Arl13B and EHD1) prompted us to study their putative function in primary cilium assembly.

Here, we describe the role of EFA6A as an essential regulator of ciliogenesis. In human cells, EFA6A is required for the removal of the ciliation inhibitor CP110, and acts together with Arf6, Arl13B and Rab8 to assemble the CV by regulating the fusion of DAVs and to promote PC elongation.

RESULTS

EFA6A is involved in ciliogenesis

We searched for a role for EFA6A in PC biogenesis using the classical hTert-RPE-1 (RPE-1) and ARPE-19 cell models of ciliogenesis. We first determined the localization of exogenous EFA6A expressed at low levels in both cell types after serum starvation to induce ciliogenesis. In addition to its established plasma membrane localization, EFA6A was detected along the entire primary cilium where it colocalized with Arl13B, a bona fide marker of the ciliary membrane (Fig. 1A). The colocalization between EFA6A and Arl13B to the cilium was observed in 56% of EFA6A transfected cells (n=100).

In RPE-1 cells, siRNA-mediated depletion of EFA6A strongly inhibited ciliogenesis, as assessed by analyzing acetylated tubulin staining (70.1% of ciliated cells in the control compared to 6.1% in EFA6A siRNA pool treated cells; Fig. 1B,C; Fig. S1A,B). Similar results were obtained using the cilia marker Arl13B (Fig. S1C,D), which confirmed that EFA6A depletion affected ciliogenesis. In contrast, EFA6A depletion did not affect the distribution of pericentriolar satellites as assessed through PCM1 staining (Fig. 1B), nor was Golgi morphology affected as indicated by p23 (also known as TMED10) labeling (Fig. S1E). These results suggest a specific role for EFA6A in the assembly of the PC.

RPE-1 cells express two other EFA6 isoforms, EFA6B and EFA6D (also known as PSD4 and PSD3, respectively) (Fig. S1A,B). Knockdown of either one had no effect on the presence or morphology of primary cilia (Fig. S1C,D). This result indicates that ciliogenesis is specifically controlled by the EFA6A isoform in RPE-1 cells.

To overcome the low transfection efficiency of GFP–EFA6A in RPE-1 cells, we performed a rescue experiment in ARPE-19 cells. We first confirmed that EFA6A was required for ciliogenesis in ARPE-19 cells (Fig. 1D,E). Importantly, expression of GFP–EFA6A resistant to siRNA-EFA6A#4 (Fig. S1F), but not the control GFP alone, significantly rescued ciliation, confirming that EFA6A was required for PC assembly (Fig. 1D,E).

To determine whether EFA6A plays a general role in ciliogenesis, we turned to the MDCK renal epithelial cell model. The exogenous and inducible expression (Tet-Off system) of a human vsv-g-tagged EFA6A significantly increased the cilium length but not the percentage of ciliated cells (Fig. 2A,B; Fig. S2A). Furthermore, the cilia elongation mediated upon EFA6A expression was also observed in MDCK cells grown in 3D culture, indicating that this stimulatory property also occurs in near physiological conditions (Fig. 2C). Finally, siRNA-mediated EFA6A depletion inhibited ciliogenesis, which was rescued by the expression of human vsv-g-tagged EFA6A resistant to the canine-specific siRNA (Fig. 2D; Fig. S2B).

Thus, EFA6A appears to act as a general regulator of ciliogenesis and controls both cilium assembly and elongation.
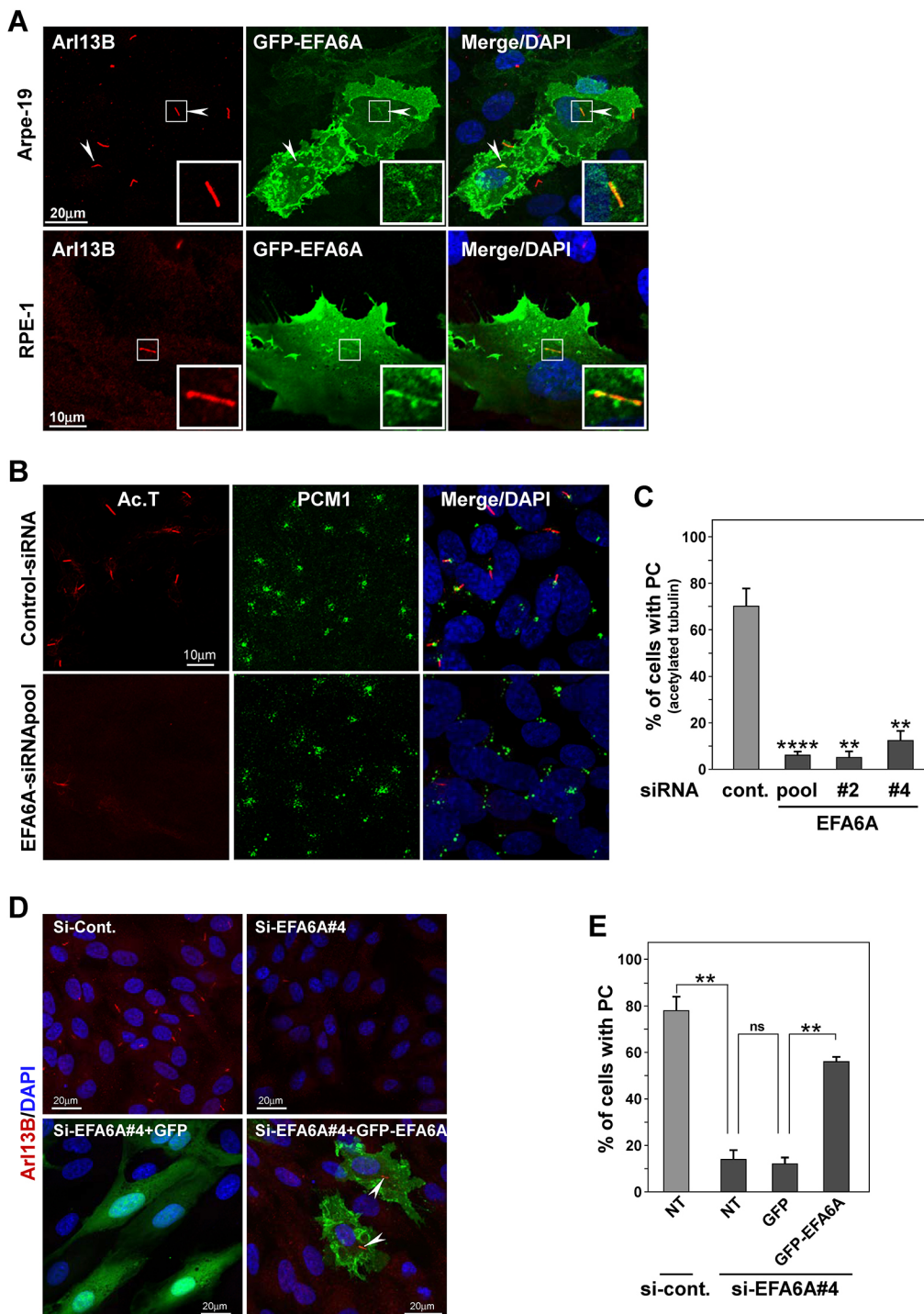
Fig. 1. EFA6A controls ciliogenesis in RPE-1 and ARPE-19 cells. (A) Localization of GFP–EFA6A transiently expressed in ARPE-19 and RPE-1 cells for 48 h, starved for 24 h and stained with anti-Arl13B antibody. (B) EFA6A depletion inhibits ciliogenesis without affecting PCM1 localization. Acetylated tubulin (Ac.T), and PCM1 were detected in control or EFA6A siRNA-treated RPE-1 cells serum starved for 24 h. (C) Ciliation quantification in 48 h siRNA-treated cells (control, EFA6A si-pool, si#2 and si#4) with 24 h serum starvation, followed by staining with acetylated α-tubulin and γ tubulin antibodies. Results are mean±s.d. from n=3 to 5 independent experiments, with >200 cells per treatment. For si-pool n=5 and P=3.2×10^{-5}; for si#2 and si#4 n=3 and P=6.3×10^{-3}, and P=6.5×10^{-3}, respectively. (D) siRNA EFA6A knockdown-rescue experiment. GFP-EFA6A expression in ARPE-19 cells rescued siRNA-mediated inhibition of ciliogenesis. Representative confocal images of ARPE-19 cells transfected or not with GFP or GFP-EFA6A expressing vectors for 24 h followed by siRNA treatment. At 48 h post-transfection, cells were serum-starved for 24 h and stained with anti-Arl13B. (E) Quantification of the percentage of ciliated cells for experiments described in (D). Results are mean±s.d. from n=3 independent experiments, with between 40 and 250 cells per treatment. For si#4 P=5.2×10^{-3}, for GFP P=0.33 and for GFP–EFA6A P=3.2×10^{-3}. **P<0.01, ****P<0.0001; ns, not significant (Student's t-test).

Arf6 is required for ciliogenesis and its active form rescues ciliogenesis impaired by EFA6A depletion

As EFA6 is known to specifically activate the small GTP-binding protein Arf6, we wondered whether this latter protein was also involved in the assembly of the PC. Arf6-depletion mediated by two different siRNA strongly inhibited ciliogenesis in RPE-1 cells (Fig. 3A,B; Fig. S2C). To complement these loss-of-function studies, we overexpressed the dominant negative Arf6T27N mutant and the fast-cycling Arf6T157N mutant that can be activated independently of the exchange factor. The expression of the dominant-negative mutant, but not of the fast-cycling mutant,

impaired ciliation (Fig. 3C,D) indicating that Arf6 is required for ciliogenesis in RPE-1 cells. We confirmed these results in MDCK cells where the inducible expression of the dominant-negative Arf6T27N, but not of the fast-cycling Arf6T157N, form inhibited PC assembly (Fig. S2D). Finally, we tested whether the expression of Arf6 fast-cycling mutant could rescue the impairment of ciliation due to EFA6 depletion. We observed that expression of Arf6T157N–mCherry, but not that of control mCherry, rescued ciliation in cells treated with EFA6A siRNA (Fig. 3E,F).

Taken together, our data demonstrate that EFA6A regulates PC assembly, at least in part, by activating the small G protein Arf6.
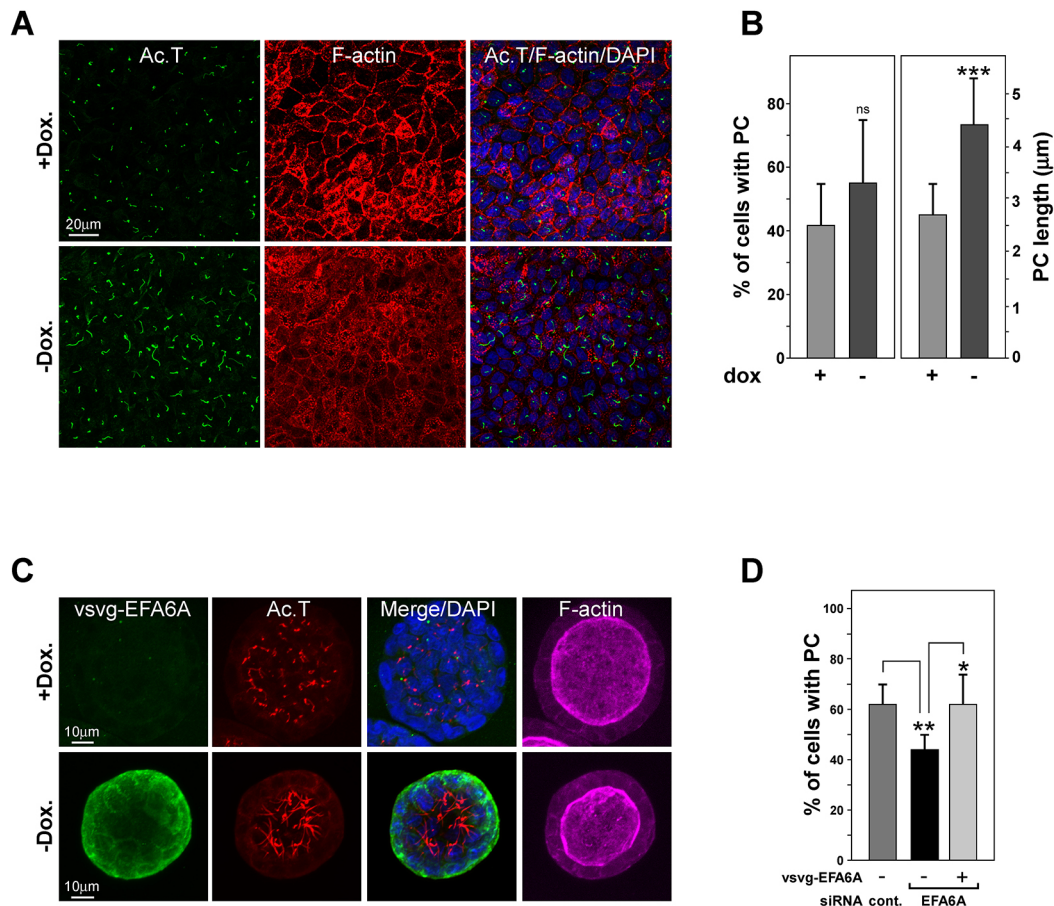
Fig. 2. EFA6A plays a role in ciliogenesis in MDCK cell model. EFA6A overexpression increases cilium length in 2D and 3D culture systems. (A) MDCK cells expressing (−dox) or not (+dox) vsv-g–EFA6A were grown on polycarbonate filters for 10 days then fixed and processed for immunofluorescence. Ac.T, acetylated tubulin. (B) Quantification of the effect of EFA6A exogenous expression on the percentage of cells with a PC and the cilium length observed in A. Mean±s.d.; between 475 and 1044 cells per sample, n=3 for Dox and n=3 for no Dox, P=0.16 (ns, not significant) for percentage of cells with a PC (cilium to nuclei number) and P=2.5×10^{-5} (***P<0.001) for average cilium length (μm). (C) EFA6A exogenous expression increases cilium size in 3D culture system. MDCK cells expressing (−dox) or not (+dox) vsv-g–EFA6A were grown in Matrigel for 7 days then fixed and processed for immunofluorescence using antibodies against vsv-g (green) and Ac.T (red), with F-actin labeled using phalloidin (magenta) and nucleus with DAPI (blue). (D) Ciliogenesis rescued with human vsv-g–EFA6A in MDCK cells treated with siRNA against canine EFA6A. MDCK cells were transfected with a control siRNA or a canine EFA6A-specific siRNA and grown on poly-carbonate filters. After 10 days, the fully polarized cells were processed for immunofluorescence and the primary cilia stained with an anti-Arl13B antibody. The experiment was performed three times and data from all three experiments were combined. An average of 4000 cells per sample was analyzed for the presence or absence of a cilium. Values are mean±s.d., n=3, t-test P=1.1×10^{-3} for siEFA6A +dox; P=0.04 for siEFA6A −dox. *P<0.05, **P<0.01.

EFA6A accumulates at the m-centriole during the initiation of PC assembly

The fact that EFA6A depletion abolished the formation of PC suggested that it might act during the early steps of ciliogenesis. We then assessed the localization of EFA6A during the induction of ciliogenesis in GFP–EFA6A-expressing ARPE-19 cells (Fig. 4A). Interestingly, before serum starvation (0 min), we observed the presence of EFA6A-positive structures, but not of Arl13B-positive structures, near the m-centriole (as labeled by CEP164) (Fig. 4A; Fig. S3). After serum starvation, these EFA6A-containing structures accumulate to the m-centriole together with newly arrived Arl13B-containing structures in order to form the PC where the two proteins localized (Fig. 4A; Movie 1).

Our data show that EFA6A is present at the CEP164-labeled m-centriole before the arrival of Arl13B-positive structures. During PC assembly, distinct structures labeled by EFA6A or by Arl13B accumulated at the m-centriole to colocalize eventually along the resulting PC.

Taken together, our result strongly suggests that EFA6A controls one of the first steps of ciliogenesis.

EFA6A depletion prevents the removal of CP110 from the m-centriole

We then investigated the molecular mode of action of EFA6A during the early steps of ciliogenesis (Fig. 4B). The CP110 protein caps the distal end of both centrioles and its removal from the m-centriole is required for the initiation of ciliogenesis (Tsang and Dynlacht, 2013). In serum-starved RPE-1 cells, EFA6A siRNA treatment significantly increased the proportion of cells containing two CP110-capped centrioles (63.4% versus 30.6% in control cells; Fig. 4Ba). This observation suggests that EFA6A depletion might block cilia formation, at least in part, by inhibiting the dissociation of CP110 from the m-centriole. CP110 removal is known to be driven by the centriole distal appendage protein CEP164 and the recruitment of the serine/threonine kinase TTBK2 to the sub-distal appendages (for a review, see Wei et al., 2015). EFA6A depletion did not inhibit the accumulation of either CEP164 or TTBK2 at the centrioles (Fig. 4Bb,Bc).

These observations indicate that EFA6A does not regulate the localization of CEP164 and TTBK2 to the m-centriole but is essential for CP110 removal.
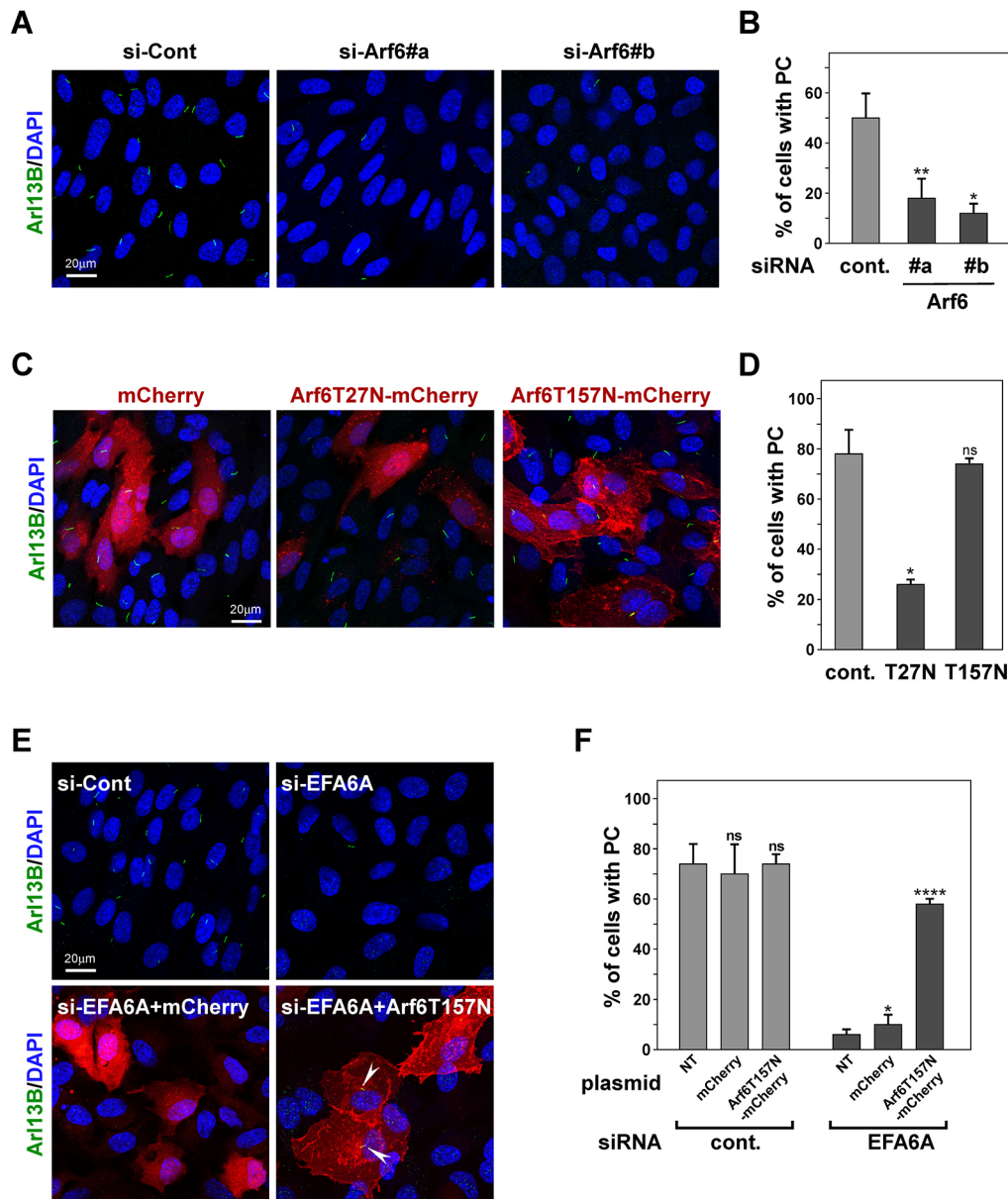
Fig. 3. Arf6 control ciliogenesis in RPE-1 cells. (A) Arf6 depletion inhibits ciliogenesis. Arl13B was detected in control or Arf6 siRNA-treated RPE-1 cells serum starved for 24 h. (B) Ciliation quantification in 48 h siRNA-treated cells (control, Arf6 si#a and si#b) with 24 h serum starvation, followed by staining with Arl13B antibodies. Results are mean±s.d. from three independent experiments, with >500 cells per treatment. For si#a $P=5.1×10^{-3}$ and si#b, $P=2.0×10^{-2}$. (C) Expression of the dominant-negative (T27N) mutant but not of the fast cycling (T157N) mutant of Arf6 inhibits ciliogenesis. Representative confocal images of RPE-1 cells transiently expressing mCherry (control), Arf6T27N–mCherry or Arf6T157N–mCherry for 48 h, starved for 24 h and stained with anti-Arl13B antibodies. (D) Quantification of the percentage of ciliated transfected cells for experiments described in C. Results are means±s.d. from three independent experiments, with ~300 cells per transfection. For Arf6T27N $P=1.3×10^{-2}$; for Arf6T157N $P=5.9×10^{-1}$. (E) Expression of the fast cycling (T157N) mutant of Arf6 in RPE-1 cells rescues siRNA-EFA6A-mediated inhibition of ciliogenesis. Representative confocal images of RPE-1 cells transfected or not with mCherry- or Arf6T157N–mCherry-expressing vectors for 24 h followed by siEFA6A treatment. At 48 h post-transfection, cells were serum starved for 24 h and stained with anti-Arl13B antibody. Arrowheads highlight the PC. (F) Quantification of the percentage of ciliated cells (NT, not transfected) or of ciliated transfected cells (mCherry and Arf6T157N–mCherry) for experiments described in E. Results are mean±s.d. from four independent experiments, with ~400 cells per treatment. For si-control, expression of mCherry and Arf6T157N–mCherry $P=6.3×10^{-1}$ and $P=9.6×10^{-1}$, respectively, and for siEFA6A, expression of mCherry and Arf6T157N-mCherry $P=2.2×10^{-2}$ and $P=1.0×10^{-6}$, respectively. $*P<0.05$, $**P<0.01$, $****P<0.0001$; ns, not significant (Student's t-test).

EFA6A depletion leads to the accumulation of Arl13B-positive distal appendage vesicles

As EFA6A is involved in membrane trafficking, we subsequently considered whether its depletion could interfere with membrane vesicle delivery to the m-centriole. Because Arl13B is a membrane ciliary marker required for ciliary membrane formation and extension, we looked for the presence of Arl13B-positive structures at the m-centrioles. Through immunofluorescence analysis, after overnight serum-starvation, we observed a typical Arl13B-decorated PC observed in control cells (Fig. 5A, left panel). In EFA6A-depleted cells, as described above, no PC was assembled. However, we observed a small but robust Arl13B-positive staining close to the CEP164-labeled m-centriole (Fig. 5A, right panel; Fig. S4). This result suggests that, even if it leads to the inhibition of
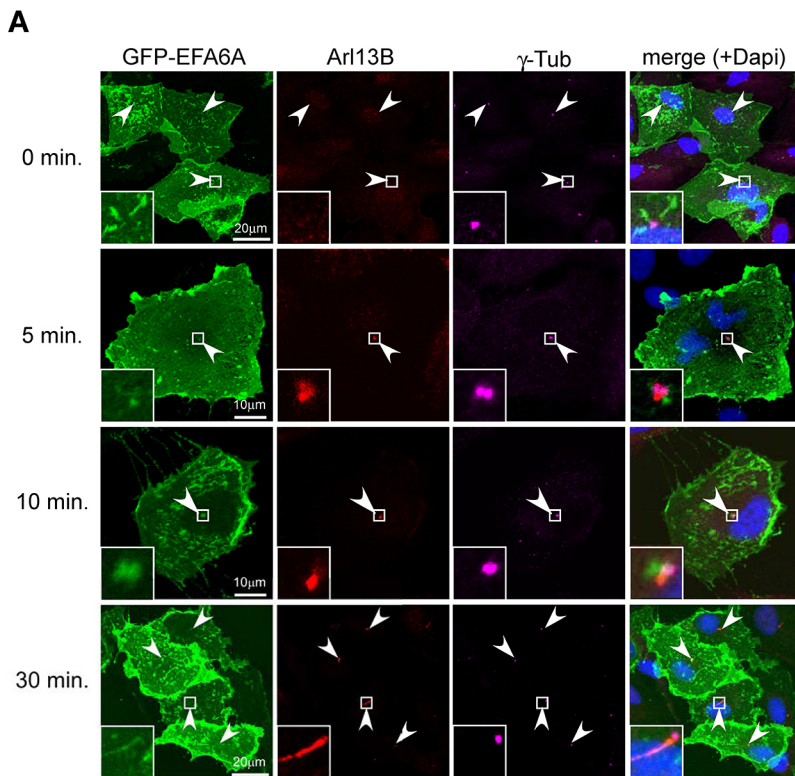
A

Fig. 4. EFA6A accumulates to the m-centriole during PC assembly and controls CP110 release. (A) ARPE-19 cells transiently expressing GFP–EFA6A were imaged at different times following serum starvation by confocal microscopy using anti-Arl13B (red) and γ-tubulin (magenta) antibodies. The arrowheads highlight the accumulation of GFP–EFA6 and/or Arl13B at one of the two centrioles. Inset shows a magnified view of indicated region. (B) EFA6A depletion prevents CP110 release from the m-centrioles (a) but does not impair the recruitment of CEP164 (b) or TTBK2 (c). γ tubulin (γ-Tub), CP110, CEP164 and TTBK2 were detected in control and EFA6A siRNA-treated RPE-1 cells with 24 h serum starvation. Results are mean±s.d. (n=3–5 independent experiments), >500 cells per treatment, P=4.9×10^{-5} for CP110, P=0.8 and 0.6 for CEP164 and TTBK2, respectively. ****P<0.0001; ns, not significant (Student's t-test).

B
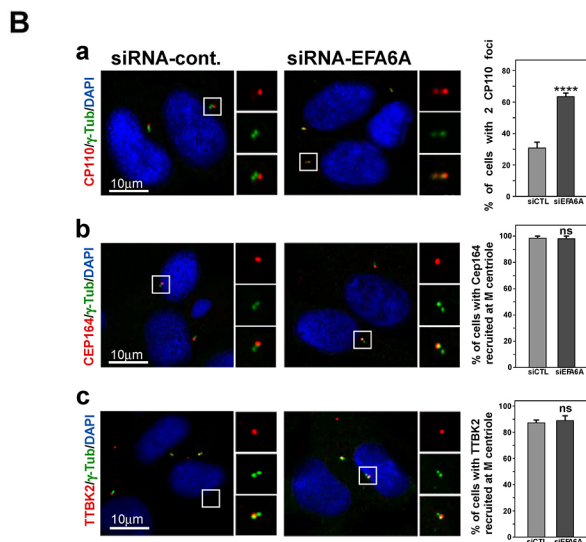
PC formation, EFA6A depletion is not preventing the formation and the docking of Arl13B-positive structures to the m-centriole.

To better characterize these Arl13B-containing structures, we used stimulated emission depletion (STED) super-resolution microscopy on serum-starved RPE-1 cells. In control cells, as expected, Arl13B was present all along the PC; however, the labeling appeared patchy along the ciliary membrane (Fig. 5B). This observation suggested that Arl13B was enriched in specific domains of the ciliary membrane. In EFA6A-depleted cells, we observed an accumulation of Arl13B-positive small vesicles around one of the two centrioles (Fig. 5B). STED 3D imaging confirmed that these Arl13B-positive structures were docked to the m-centrioles very close to the ring-shaped centriolar CEP164 protein complex (Fig. 5C; Movie 2).

To bear out the presence of small vesicles surrounding the m-centriole, we carried out electron microscopy (EM) studies on serum-starved RPE-1 cells (Fig. 5D). Control cells exhibited a typical PC (Fig. 5Da) comprising a basal body with distal appendages and a long axoneme surrounded by a proximal part of the ciliary pocket (Ghossoub et al., 2011). In contrast, EFA6A-depleted cells rarely exhibited apparently normal fully assembled cilia or CV-docked basal bodies. In most of the cells, small vesicles (between 50 and 100 nm diameter) were found very close to the m-centrioles, likely docked to the distal appendages confirming STED imaging (Fig. 5Db; see Fig. 6G for quantification). Serial-section transmission electron microscopy (∼70 nm per slide) demonstrated that these structures were small vesicles as most of these membrane structures were lost between two sections
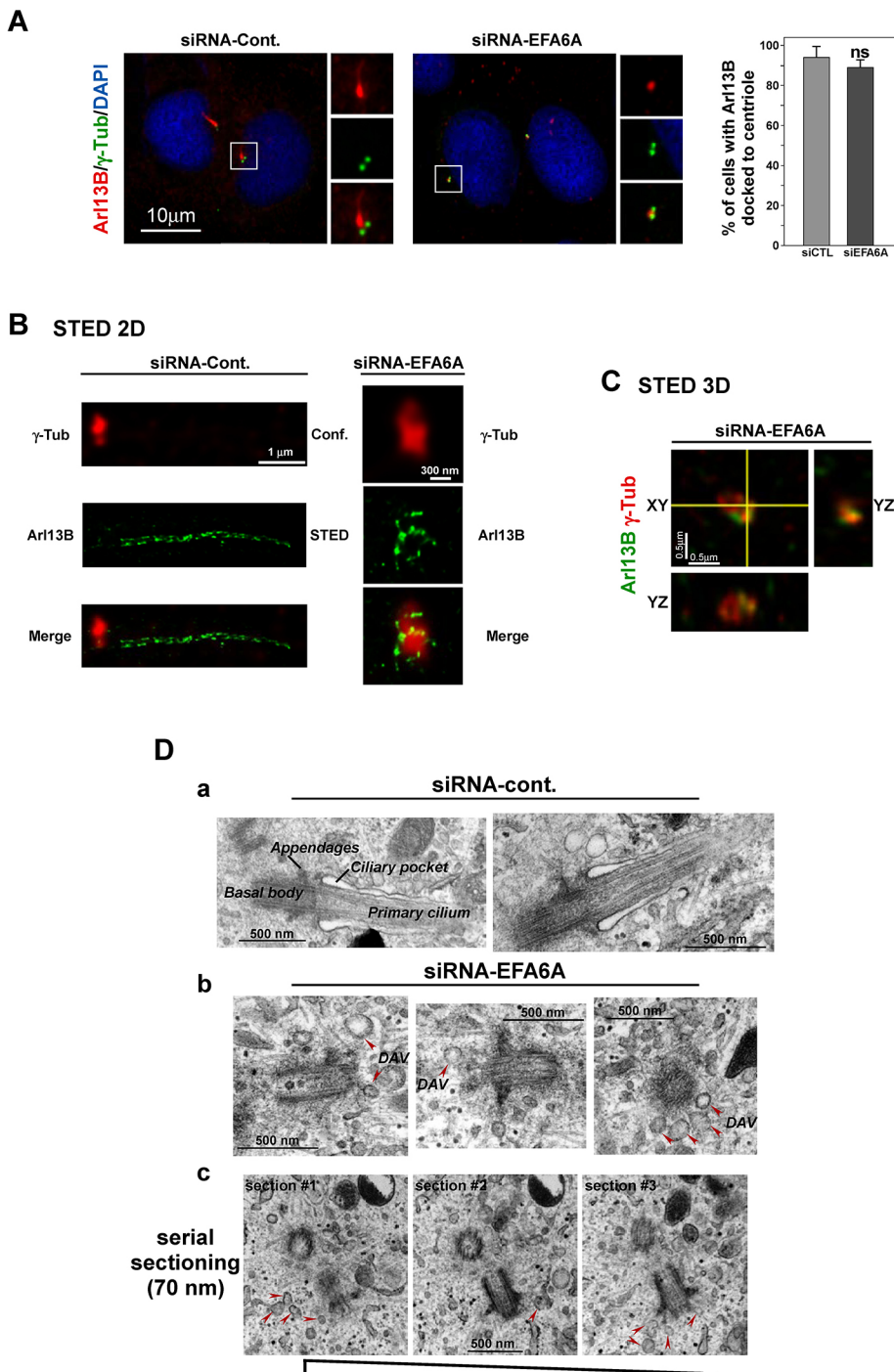
Fig. 5. Knockdown of EFA6A inhibits the assembly of the CV and leads to the accumulation of DAVs. (A) EFA6A depletion does not prevent the accumulation of Arl13B-positive structures at the centriole. γ-tubulin (γ-Tub) and Arl13B were detected and imaged by confocal microscopy in control or EFA6A siRNA-treated RPE-1 cells after 24 h serum starvation. Results are mean±s.d. (*n*=3–5 independent experiments), >400 cells per treatment, *P*=0.3 (ns, not significant). (B,C) Visualization of DAVs by 2D STED super-resolution microscopy (B) and 3D STED (orthogonal view) (C). γ-Tub and Arl13B were detected and imaged by STED microscopy in control or EFA6A siRNA treated RPE-1 cells for 48 h with serum starvation for the last 24 h. (D) Visualization of DAVs by TEM. Representative electron micrographs of RPE-1 cells treated with siRNA control (a) or EFA6A pool (b,c) for 48 h with serum starvation for the last 24 h. Serial TEM images of siRNA-EFA6A treated RPE-1 cells are shown in c. DAVs are highlighted.

(Fig. 5Dc). These vesicles are reminiscent of m-centriole-docked DAVs prior to their fusion to form CV (Lu et al., 2015b).

Collectively, our data demonstrate a key role for EFA6A in the formation of the ciliary vesicle by regulating the fusion of the DAVs.

Arl13B interacts with EFA6A and partially rescues the inhibition of PC formation upon EFA6A depletion

We then looked for a physical link between EFA6A and Arl13B. Using GST pulldown experiments, we demonstrated that full-length EFA6A, and to a lesser extent its catalytic Sec7 and PH domains, were able to specifically bind Arl13B–GFP from ARPE-19 and

BHK cell lysates (Fig. 6A,B). The interaction was not limited to the isoform EFA6A as Arl13B also pulled down EFA6B (Fig. S5A). Using purified proteins, we demonstrated that EFA6A interacted directly with Arl13B and preferentially with the active GTP-bound form (Fig. S5B). Finally, EFA6A did not act as an Arl13B–GEF (Fig. S5C). Taken together, these results indicate that EFA6A and the active form of Arl13B could function together within the same complex.

Thus, we analyzed the effect of Arl13B depletion on ciliogenesis and observed that, as previously described (Larkins et al., 2011; Li et al., 2016), and similar to what was seen upon EFA6A depletion, it strongly inhibited RPE-1 ciliation (Fig. 6C; Fig. S5D,E). Next, we
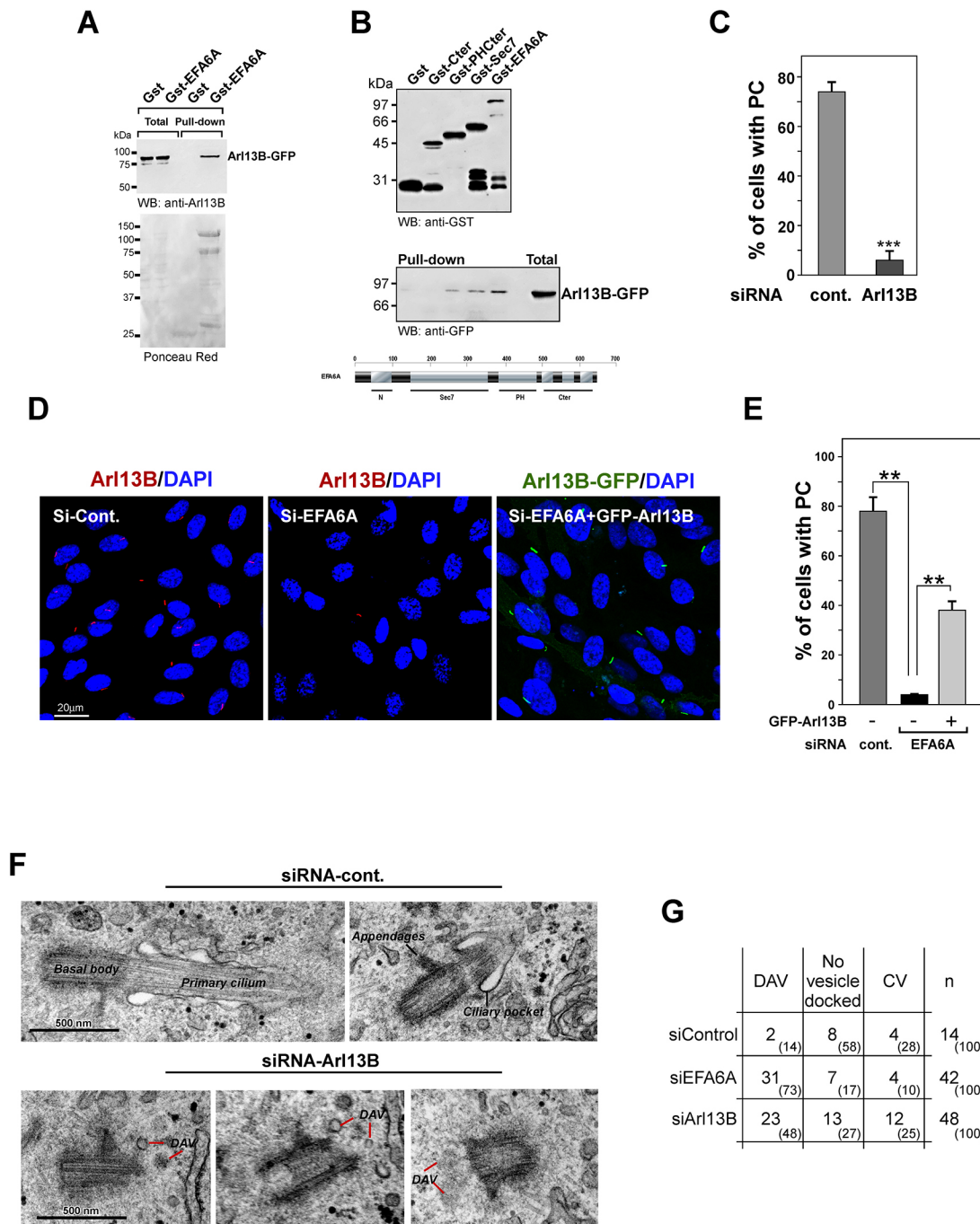
Fig. 6. Arl13B interacts with and acts downstream of EFA6A. (A) GST pulldown of Arl13B–GFP expressed in ARPE-19 cells by EFA6A fused to GST. WB, western blotting. (B) GST pulldown of Arl13B–GFP expressed in BHK cells with different constructs of EFA6A fused to GST. The domain organization of EFA6A is represented underneath. (C) Analysis of the effect of Arl13B depletion on ciliogenesis. RPE-1 cells were transfected with siRNA control or siRNA pool against Arl13B for 48 h, with 24 h serum starvation, followed by staining with acetylated α-tubulin antibodies. Quantification of ciliation is shown here. Means±s.d. from three independent experiments, with an average of 400 cells per sample analyzed for the presence or absence of a cilium, t-test. $P=2.9\times10^{-4}$ for siArl13B. (D) Overexpression of Arl13B–GFP partially rescued the inhibition of ciliogenesis induced by EFA6A depletion. RPE-1 cells were transfected or not with pEGFP-Arl13B for 24 h and then transfected with siEFA6A for 48 h, with 24 h serum starvation, followed by staining with acetylated tubulin or Arl13B antibodies. (E) Quantification of ciliation is shown. Results are mean±s.d., $n=3$ independent experiments, >500 cells per sample analyzed for the presence or absence of a cilium. $P=1.9\times10^{-3}$ for siEFA6A pool treated sample and $P=5.7\times10^{-3}$ for the siEFA6A pool-treated and Arl13B-GFP-expressing sample. (F) Representative electron micrographs of RPE-1 cells treated with siRNA control or Arl13B pool for 48 h with serum starvation for the last 24 h. (G) Quantification of electron microscopy experiments. Only m-centrioles without elongated cilia are quantified (i.e. ~30% of control cells and ~90% of the siEFA6A and siArl13B cells as determined by immunofluorescence experiments). Values in brackets represent percentages. **$P<0.01$, ***$P<0.001$ (Student's t-test).

performed rescue experiments to determine the functional link between EFA6A and Arl13B. EFA6A overexpression could not rescue the inhibition of ciliogenesis caused by Arl13B depletion (Fig. S5E). In contrast, expression of Arl13B–GFP partially rescued the inhibition of ciliogenesis upon EFA6A depletion (Fig. 6D,E). These results indicate that Arl13B acts downstream of EFA6A in PC assembly.

Thus, we postulated that EFA6A might form a complex with Arl13B to promote the fusion of the DAVs, in which case the depletion of Arl13B, similar to what is seen upon EFA6A depletion, should lead to inhibition of CV formation and the presence of DAVs near m-centrioles. Indeed, EM imaging showed that Arl13B depletion resulted in a majority of m-centrioles becoming surrounded with small membrane vesicles (Fig. 6F,G). However, we noticed that in 25% of the Arl13B-depleted cells a CV was still present, suggesting that the formation of the CV does not require high amounts of Arl13B or that another protein could partially compensate for the absence of Arl13B to mediate the fusion of the DAVs.

Our results indicate that EFA6A interacts with Arl13B to assemble the PC through the fusion of DAVs to form the CV.

EFA6A interacts with Rab8 and is required to localize Rab8-positive structures to the m-centriole

Since Rab11 and Rab8 are essential for PC formation and to mediate vesicular transport to the ciliary base, we asked whether EFA6A could have a role in the Rab11/Rab8 pathway. We first analyzed the effect of EFA6A depletion on the localization of Rab11 and Rab8

GFP-fused proteins in serum-starved ARPE-19 cells. As expected, in control cells (siRNA control), Rab11-positive structures were present in the vicinity of the m-centriole (Fig. 7A, upper panels), whereas Rab8 was enriched all along the PC (Fig. 7C, upper panels). In EFA6A-depleted cells, Rab11-containing structures were still present (Fig. 7A, lower panels). In contrast, Rab8 staining in close contact with the centrioles disappeared in the majority of EFA6A-depleted cells (Fig. 7C, lower panels; see Fig. 7B,D for quantifications). This observation suggests that EFA6A might be required for the recruitment of Rab8-containing vesicles to the m-centriole. This is supported by the finding that GST–EFA6A specifically pulled down Rab8–GFP but not Rab11–GFP from an ARPE-19 cell lysate. These results indicate that EFA6A regulates the Rab8-dependent function along the Rab11 and Rab8 cascade.

DISCUSSION

Biogenesis of the PC is an important and intricate process that has been the object of numerous studies. The hierarchical series of events converting the m-centriole to a fully formed cilium have been well established, yet the detailed molecular mechanisms and the
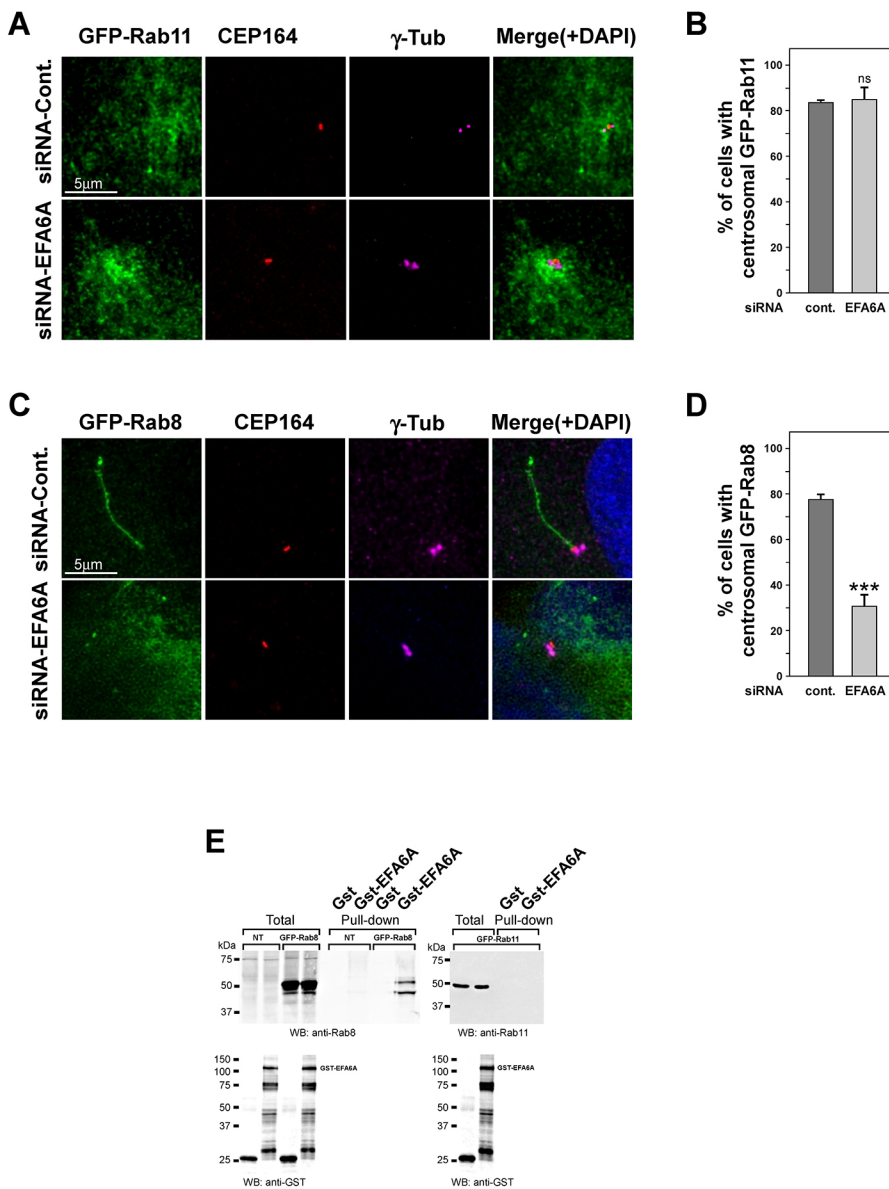

Fig. 7. EFA6A is required for centrosomal accumulation of GFP–Rab8-positive structures. ARPE-19 cells were transiently transfected with GFP–Rab11 (A) or GFP–Rab8 (C) expression vectors for 24 h before siRNA (control or EFA6A pool) treatment. At 48 h post-transfection, cells were serum starved for 12 h and stained with anti-CEP164 and anti-γ-tubulin antibodies. Representative confocal images deconvolved using Huygens Professional, using the CMLE algorithm, with, SNR:20 with 40 iterations are shown. Quantification of ciliary or centrosomal accumulation of GFP–Rab11 (B) or GFP–Rab8 (D) structures. Results are mean±s.d., n=2 for B and 4 for D; >40 cells per sample were analyzed, t-test P=0.7 for siEFA6A pool treated GFP–Rab11-expressing cells and P=2.0×10^{-4} for siEFA6A pool treated GFP–Rab8-expressing cells. (E) GST–EFA6A pulled down GFP–Rab8 but not GFP–Rab11 expressed in ARPE-19 cells. WB, western blotting. ***P<0.001; ns, not significant (Student's t-test).

different partners involved in each step are not fully described. Here, we identify a novel molecular cascade, involving the intracellular transport regulator EFA6A, that controls primary cilium formation and length.

A role for EFA6A in CV formation and CP110 release

EFA6A depletion in MDCK, RPE1 and ARPE-19 cell models abolished the formation of PC induced by serum starvation. This demonstrates a conserved and essential role of EFA6A in ciliogenesis. Interestingly this role is only carried out by the EFA6A isoform, indicating that it has very specific cellular role(s). EFA6A is a specific and potent Arf6 exchange factor. Here, we demonstrate that its catalytic activity is required for PC assembly. Indeed, Arf6 depletion, as well as expression of a dominant-negative Arf6 mutant, inhibits ciliogenesis. In addition, overexpression of a constitutively active mutant of Arf6 at least partially recues the lack of PC assembly induced by EFA6A depletion. Thus, EFA6A is involved in ciliogenesis mainly by controlling Arf6 activation. However, as the siRNA-mediated depletion of EFA6A is not total, we cannot state that activated Arf6 mediates all the putative functions of EFA6A in ciliogenesis or rule out that residual EFA6A in combination with a high amount of activated Arf6 may be required to rescue ciliogenesis.

Our data show that EFA6A is required to remove the negative regulator of ciliogenesis CP110 from the m-centriole and is thus indispensable in the early stages of ciliogenesis. The persistence of CP110 could explain the absence of ciliogenesis in EFA6A-depleted cells. However, EFA6A depletion did not affect the recruitment of CEP164 or the kinase TTBK2 to the basal body, two proteins required for the removal of CP110. These results suggest that EFA6A could either regulate the kinase activity of TTBK2 or control the release of CP110 through an unknown mechanism (see below).

Immunofluorescence analyses in EFA6A-depleted cells revealed the accumulation of small Arl13B-positive structures in the vicinity of the centrioles. Super resolution microscopy and EM studies confirmed the presence of small vesicles (DAVs) docked or very close to the m-centrioles and the absence of CVs. These results indicate (1) that docking of DAVs to the distal appendages of the m-centriole is not an EFA6A-dependent process, and (2) that the fusion of the DAVs into a larger CV requires EFA6A. We found that EFA6A depletion could be partially bypassed by overexpression of Arl13B but not the contrary. Indeed, we showed that the depletion of Arl13B, which also led to an inhibition of ciliogenesis in a similar manner to EFA6A, could not be rescued by EFA6A overexpression. This observation suggests that EFA6A may act upstream of Arl13B. Whereas EFA6A is mainly found at the plasma membrane, we observed that a small fraction of the protein localized near the m-centriole even in the absence of a PC (in proliferative medium conditions). At this stage, no Arl13B-positive structure is visible, indicating that EFA6A is chronologically present before Arl13B at the m-centriole. Serum starvation induces the arrival of Arl13B structures at the m-centriole, which colocalize with those of EFA6A and is concomitant with PC assembly. These observations are consistent with a role of EFA6A to recruit and promote the fusion of Arl13B structures to assemble the PC, where eventually the two proteins accumulate. In line with this hypothesis, we have discovered a direct interaction between EFA6A and Arl13B. Interestingly, we have not been able to observe an interaction between Arf6 and Arl13B, suggesting that EFA6A regulates the fusion of the DAVs by both activating Arf6 and recruiting Arl13B.

Arl13B, EFA6 and Arf6 all regulate the endocytic recycling pathway (Barral et al., 2012; D'Souza-Schorey et al., 1995;

Decressac et al., 2004; Montagnac et al., 2009; Radhakrishna and Donaldson, 1997). Moreover, Arf6 regulates the post-endocytic recycling through its interaction with Sec10 (Prigent et al., 2003). Here, we demonstrate that activation of Arf6 is required for PC assembly. Thus, we propose that, during ciliogenesis, EFA6A could control the fusion of vesicular membranes via the recruitment of Arl13B, the activation of Arf6 and the formation of a complex including Arf6, Arl13B and the exocyst. Further experiments will be necessary to test this hypothesis.

Other proteins involved in the endocytic recycling pathway, EHD1 and EHD3, have been found to be necessary for CV assembly (Lu et al., 2015b). Much like EFA6A, EHD1 appears to be essential for both the fusion of the DAVs and the removal of CP110. Thus, the release of CP110 would be a general consequence of the inhibition of the fusion of DAVs to form the CV. In any case, it suggests the existence of an unexpected link whereby the fusion of the DAVs and the assembly of the CV can control the CP110 release from the m-centriole, a crucial step for the subsequent elongation of the axoneme. Lu et al. proposed that EHD1 and EHD3 regulate the fusion of the DAVs through SNAP29, a SNARE membrane fusion regulator. Interestingly EHD1, EFA6 and Arf6 have been implicated in the recycling of MHC-I and β1 integrin from tubular endosomes to the plasma membrane suggesting that these proteins could be part of the same vesicular transport machinery (Caplan et al., 2002).

A role for EFA6A in the Rab11 and Rab8 pathway

It has been known for many years that the Rab11/Rabin8/Rab8 cascade is involved in ciliogenesis and more precisely in the delivery of vesicular membrane during ciliogenesis (reviewed in Das and Guo, 2011; Deretic, 2013). The Rab11-dependent transport and activation of Rabin8, the Rab8 activator, from the recycling endosomes to the pericentriolar compartment, is required for the activation of Rab8 and the fusion of Rab8-positive structures to the CV. The fusion of Rab8 vesicles to the CV then contributes to the PC membrane and the extension of the cilium (Lu et al., 2015b).

Here, our data suggest that EFA6A is required for recruiting Rab8-containing structures to the m-centriole. Indeed, EFA6A depletion led to the absence of Rab8-positive vesicles at the pericentriolar region without affecting the distribution of Rab11-positive membrane structures. Knodler et al. observed that the expression of dominant-negative Rab11 in RPE-1 cells leads to an inhibition of ciliogenesis (Knodler et al., 2010). Interestingly, they did not observe a loss of Rab8 staining along the shorter cilium. They conclude that additional factors to Rab11 regulate the ciliary localization of Rab8. Our observations that GST–EFA6A specifically interacts with Rab8, and that EFA6A is required for the accumulation of Rab8-positive structures at the centriole suggest that EFA6A might be one of the factors recruiting Rab8.

We observed that the pericentriolar localization of Rab11 structures was not dependent on EFA6A. Thus, Rab11 could either act upstream of EFA6A or the two proteins could have independent roles.

EFA6A expression regulates the PC length

Analogous to its role in DAV fusion and CV formation, we propose that EFA6A-mediated membrane vesicle fusion plays a major role in PC length regulation. It is noteworthy that the overexpression of EFA6A (this study), as observed for Arl13B and Rab8 (Lu et al., 2015a; Zuo et al., 2009), increases the cilium length. One can speculate that EFA6A, Arl13B and Rab8 regulate the delivery of membranes through the recruitment, docking and fusion of membrane vesicles to the base of the growing cilia where the

exocyst complex has been found to be enriched (Seixas et al., 2016). We observed that in the absence of EFA6A, Arl13B-positive, but not the Rab8-positive, vesicles were still present in the vicinity of the m-centriole, suggesting that the centrosomal localization of Arl13B vesicles is not dependent on EFA6A. This also indicates that Arl13B vesicles arrive to the m-centriole prior to the Rab8 ones. In conclusion, we propose that EFA6A is essential at the onset of the CV assembly to mediate the fusion of Arl13B vesicles, and later is needed to recruit Rab8 vesicles that contribute to PC extension.

Is loss of EFA6A function a cause of ciliopathy?

Although ciliopathies are individually relatively rare disorders [the incidence of individual ciliopathies ranges from around 1 in 1000 for autosomal dominant polycystic kidney disease to 1 in 150,000 (Tobin and Beales, 2009)] taken as a group their high frequency has a significant impact on human health. In the absence of effective treatments, they remain a serious public health challenge. Mutations in genes that encode cilia components account for most of ciliopathies. Here, we have observed that the exogenously expressed EFA6A is localized throughout the PC in RPE-1 and ARPE-19 cell lines. In addition, we demonstrated that EFA6A plays an essential role in its assembly. Moreover, EFA6A has also been identified in a proteomic analysis of the mouse photoreceptor sensory cilium complex (Liu et al., 2007). The outer segment (OS) of photoreceptor cells is a highly specialized PC that converts light signals into an electrical output in a process called phototransduction. We predict that strong alterations in the EFA6A (*PSD*) gene post-transcriptional gene regulatory mechanisms affecting the cellular expression level of EFA6A protein could lead to ciliopathies and also retinal ciliopathies. In fact, given that the molecular mechanisms of primary cilium assembly are highly conserved, we predict that *PSD* gene mutations will be the source of pleiotropic disorders.

MATERIALS AND METHODS
Antibodies and reagents

Mouse monoclonal antibodies (mAb) against the vsv-g epitope (clone P5D4, 1:200, Roche Diagnostics GmbH, Mannheim, Germany), Sec10 (1:400, Cat. number sc-514802, Santa Cruz Biotechnology), α-Tubulin (1:1000), γ-Tubulin (1:1000), acetylated-Tubulin (1:1000) (Cat. numbers T3526, T5326, T7451, respectively, Sigma Chemical St. Louis, MO), Arf6 (clone 8A6-2, a gift from Dr Sylvain G. Bourgoin, Laval University, Quebec, Canada), Rab8 (1:1000) and Rab11 (1:1000) (Cat. Number 610844 and 610656 respectively, BD Biosciences) were used. Rabbit antisera against Arl13B (1:500) and CP110 (1:300) (Cat. numbers 17711-1-AP and 12780-1-AP, respectively, Proteintech Europe, Manchester, UK), EFA6B (1:200), TTBK2 (1:100) and CEP164 (1:300) (Cat. numbers HPA034722, HPA018113, HPA037606, respectively; Sigma), p23 (1:100), a gift from Robert G Parton (University of Queensland, St Lucia, Australia), and PCM1 (1:100, Cat. number ab154142, Abcam) were used. Fluorescent conjugated secondary antibodies from donkey and cross absorbed for the other species were from Jackson ImmunoResearch (West Grove, PA) or Molecular Probes (Invitrogen, Cergy Pontoise France). DAPI was from Sigma. Fluorescently labeled phalloidin was from Molecular Probes. Purified rabbit anti-EFA6A antibodies were prepared against a C-terminal peptide (LQPKPSSQPRAQRHS) (Eurogentec).

DNA constructs

Plasmids encoding vsv-g-tagged EFA6A, EGFP–EFA6A, His–EFA6A, His–EFA6AΔN, GST–EFA6A-Sec7, GST–EFA6A, GST–EFA6A-Cter, GST–EFA6A-PHCter, Arf6T27N–mCherry, Arf6T157N–mCherry and Arf6–His have been described elsewhere (Macia et al., 2008). Plasmid encoding Arl13B-EGFP (Hori et al., 2008) and plasmid encoding *Chlamydomonas reinhardtii* Arl13B18-278 (CrArl13B18-278) fused to GST and called GST-Arl13B(18-278) in the text, was kindly provided by Alfred Whittinghofer and Carolin Koerner (MPI Dortmund, Germany).

Plasmids encoding Rab8a–EGFP and Rab11a–EGFP were kindly provided by Drs Bruno Goud and Jean Salamero (Institut Curie, Paris, France).

Expression and purification of recombinant proteins

For the *in vitro* binding assays, recombinant Arf6 wild-type with a C-terminal hexa-His tag (Arf6–His) and recombinant N-terminal His-tagged EFA6AΔN (His–EFA6AΔN) were produced in *Escherichia coli* and purified on Ni-NTA resin according manufacturer's instructions (Qiagen). The different GST fusion proteins were also produced in *Escherichia coli* and purified by affinity chromatography on glutathione Sepharose beads (GE Healthcare). After elution with glutathione, the purified proteins were dialysed against 20 mM Tris-HCl pH 8.0, 100 mM NaCl, 1 mM MgCl$_2$, 1 mM DTT and 10% glycerol (dialysis buffer), and stored at −80°C.

GST pulldown experiments were performed with the homologous *C. reinhardtii* (Cr) Arl13B proteins purified from *E. coli*, owing to its better stability and purity. We thus prepared GST–CrArl13B(18-278).

Cell culture

All cell culture reagents were from Invitrogen/Thermo Fisher Scientific, unless otherwise indicated. Filtered fetal bovine serum (FBS) was from Perbio Thermo Scientific. All cell lines were grown in 10% FBS at 37°C in a 5% CO$_2$ incubator. ARPE-19 and RPE-1 cells (from ATCC) were cultured in DMEM/F12 (1:1). To induce cilia formation, ARPE-19 and RPE-1 cells were serum deprived overnight (unless otherwise stated) before fixation. Baby hamster kidney cells (BHK-21) were grown in BHK-21 medium (Gibco-BRL), containing 5% FCS, 10% tryptose phosphate broth, 100 U/ml penicillin, 100 mg/ml streptomycin and 2 mM L-glutamine.

MDCKII cells stably expressing vsvg-tagged EFA6A, Arf6T27N–HA and Arf6T157N–HA under the control of the tetracycline-repressible transactivator were grown in MEM (Sigma), 5% de-complemented FCS (Biowest-Abcys), penicillin-streptomycin 100 U/ml and 100 μg/ml (Klein et al., 2008; Luton et al., 2004) When indicated cells were grown on transparent permeable filters (Costar, Corning, NY) at $2{\times}10^5$ cells/12 mm filter. For 3D cell culture, cells were grown in Matrigel (BD Biosciences, San Jose, CA); $2{\times}10^3$ cells were mixed with 20 μl of Matrigel and deposited as a drop on a 12 mm glass coverslip placed in a 24-well plate and fed with regular medium.

siRNAs and mammalian expression constructs

siRNA duplexes (SiGenome smart pool) targeting human Arl13B, Sec10 (ExoC5), EFA6A, EFA6B and EFA6D and the four individual siRNA-EFA6As were purchased from Dharmacon. For EFA6A the four individual sequences of the smart pool were: siRNA#1, 5′-AGACGGAGCCUCAA-GAAUGC-3′; siRNA#2, 5′-GGGCAUGACUCUGGAACCAA-3′; siRNA#3, 5′-CCAAAUGGGAAUUCUUCUA-3′; and siRNA#4, 5′-GG-UGCUACCGCGGACUGA-3′. The control siRNA (si-cont) was from Sigma. The siRNA#2661 (5′-CCUAUCAGAGGCGGAGCUA-3′) targeting the canine EFA6A transcript was from Eurogentec. siRNAs targeting human Arf6 were: #a, 5'-CGGCAUUACUACACUGGGA-3'; and #b, 5′-A-CGUGGAGACGGUGACUUA-3′ (Sigma). Small siRNA targeting mouse EFA6A for intravitreal injection were: siRNA#1, 5′-CCAAGUGGGAA-UUCUU-3′; siRNA#2, 5′-GGUGCUACCGAGAGAC-3′ (Eurogentec).

siRNA transfection in RPE-1 and ARPE-19 cells was performed using RNAiMAX (Invitrogen) following the manufacturer's instructions and the transfected cells were incubated for 3 days at 37°C. siRNA transfection in MDCK cells was performed by nucleofection (AMAXA, Lonza Group Ltd, Switzerland) according to the manufacturer's instructions. cDNA transfections in RPE-1 and ARPE-19 cells were performed with Lipofectamine 2000 (Invitrogen), in BHK cells were performed with Jet-PEI (Polyplus transfection, Illkirch, France) and in MDCK cells were performed by nucleofection (AMAXA, Lonza Group Ltd, Switzerland). The transfected cells were incubated for 24 h or 48 h at 37°C. All cDNAs were amplified in DH5α *Escherichia coli* (Invitrogen) and prepared following the manufacturer's instructions (Qiagen).

RNA isolation, RT-PCR and qRT-PCR

Total mRNA was isolated according the Chowynski method using Fast Prep apparatus (Q-Biogen). 2 μg of total RNA was denatured at 65°C for 10 min

11

and incubated for 1 h at 50°C in presence of 2.5 mM dNTP, 100 U Superscript III (Invitrogen) using 0.5 µg oligo(dT)$_{15}$ primer in a total volume of 20 µl, followed by an inactivation step of 15 min at 70°C. A negative control lacking RT enzyme was also performed in each assay (NRT).

PCR was performed with mouse EFA6A (forward) 5′-ATCTCTGTTG-CGCCCC-3′, (reverse) 5′-GGGCGGCGGAAGCCCTGA-3′ and GAPDH (forward) 5′-GAACATCATCCCTGCATCC-3′, (reverse) 5′-CCAGTGA-GCTTCCCGTTCA-3′ primers with HotStartTaq DNA polymerase according to the standard protocol described by the manufacturer (Q-Biogen). The PCR products obtained after 35 cycles were separated through a 1% agarose gel, visualized under UV after staining with ethidium bromide. The PCR fragments of expected sizes for EFA6A and GAPDH mRNA-derived PCR products were obtained.

Quantitative real-time PCR (qRT-PCR) was carried out with The LightCycler® 480 SYBR Green I Master (Roche Life Science) in triplicate and analyzed using LightCycler® 480 Software, Version 1.5 (Roche). Primers sequences were as follows: human EFA6A, forward 5′-AGGGCATGATCCTCTACCTG-3′ and reverse 5′-ATGCTGATGGCAT-TCTTGAG-3′; canine EFA6A, forward 5′-CAACGGGCAGAAAGCAG-ACC-3′ and reverse 5′-CTTGAGGTACTCGCCAGCCA-3′; human EFA6B, forward 5′-AGCTGGAAAGTGAGCCAGAT-3′ and reverse 5′-CAGCAGATGGAGTGTGGTTT-3′; human EFA6D: forward 5′-AAGG-CCTTGTCTGAAGAGGA-3′ and reverse: 5′-CTCTGGGCTCTGAGTT-TGAA-3′; human/canine GAPDH, forward 5′-TGCCTCCTGCACCA-CCAACT-3′ and reverse 5′-CCCGTTCAGCTCAGGGATGA-3′.

The expression of each gene was normalized to that of the *GAPDH* housekeeping gene, and relative levels were calculated on the basis of the comparative cycle threshold Ct method ($2^{-\Delta\Delta Ct}$) where $\Delta\Delta Ct$ is the difference in Ct between target and reference gene.

Western blot analysis
Cells were washed twice in PBS then scrapped and resuspended in lysis buffer (20 mM triethanolamine pH 8.0, 150 mM NaCl, 5 mM EDTA, 0.5% SDS and protease inhibitor PMSF 0.25 mM). Cell lysates were centrifuged and supernatants were diluted with Laemmli sample buffer. The proteins were heat denatured and processed by SDS-PAGE, transferred to nitrocellulose membranes, stained with Ponceau Red and immunoblotted with the indicated antibodies. Proteins were detected with SuperSignal western lightning chemiluminescence reagents (ThermoScientific) following the manufacturer's instructions.

GST pulldown experiments
ARPE-19 or BHK cells were transfected or not with plasmid encoding GFP–Arl13B, Rab8–GFP and Rab11–GFP using Jet-PEI. After 24 h, cells were lysed in 50 mM Tris-HCl pH 8.0, 100 mM NaCl, 10 mM MgCl$_2$, 10% glycerol, 1% Triton X-100, 2 mM DTT and a cocktail of protease inhibitors (Roche, Diagnostics GmbH, Mannheim, Germany), and centrifuged at 15,000 *g* for 10 min at 4°C. Supernatants were incubated with 0.5 µM GST constructs in the presence of 0.75% BSA and glutathione–Sepharose beads for 4 h at 4°C.

For the direct binding assay with purified recombinant proteins, 0.2 µM His–EFA6A was incubated in 50 mM Tris-HCl pH 8.0, 100 mM NaCl, 10 mM MgCl$_2$, 10% glycerol, 2 mM DTT and a cocktail of protease inhibitors with 0.5 µM GST or GST–Arl13B in the presence of 0.75% BSA and glutathione–Sepharose beads for 1 h at 25°C.

Beads were washed, and bound proteins were eluted using SDS sample buffer and separated by SDS-PAGE. Their presence in the eluate was detected by western blotting using the anti-tag antibodies.

Rescue experiments
For EFA6A rescue experiments, we used the plasmid containing EGFP–EFA6A, which is resistant to siRNA-EFA6A #4. Indeed, the siRNA#4 targets (in position 881 of the nucleotide sequence) the large N-terminal domain present in the 110 kDa (1024aa/3072 bp) EFA6A isoform (human PSD NM_00277 9), but absent in the shorter 72 kDa (645aa/1938 bp) isoform as described in Franco et al. (1999). We cloned and inserted the shorter isoform in the pEGFP vector.

The rescue construct or control vector (EGFP or mCherry) was transiently transfected into ARPE-19 or RPE-1 cells 24 h prior to the transfection of the cells with the different siRNA. After 48 h, cells were serum-starved for 24 h fixed and processed for immunofluorescence analysis.

[35S]GTPγS-binding assay
Arf6–His or GST–Arl13B (2 µM) were incubated at 30°C with [^{35}S]GTPγS (20 µM, ~2000 cpm/pmol) in 50 mM HEPES (pH 7.5), 2 mM MgCl$_2$, 100 mM KCl, with azolectin (2 mM), and with or without (as indicated in the figure legend) His-tagged EFA6A (0.5 µM). At the indicated times, samples of 25 µl were removed and measured for radioactivity as described previously (Franco et al., 1999).

Preparation of phospholipid vesicles
Large unilamellar vesicles of azolectin were prepared as previously described (Franco et al., 1995), and extruded through a 0.4 µM pore size polycarbonate filter (Isopore, Millipore).

Immunofluorescence and confocal microscopy analysis
Cultured cells were fixed on 11 mm round glass coverslips with 3% paraformaldehyde and processed for immunofluorescence analysis as described previously (Franco et al., 1998). Confocal microscopy analysis was carried out with a Leica TCS-SP5 microscope (Leica Microsystems) or a LSM-780 (Zeiss). Images were analyzed using Image J and Adobe Photoshop software.

For centrosomal markers, the cells were fixed in methanol at −20°C for 4 min, rinsed twice in PBS and processed as above.

STED microscopy
All samples were mounted in Abberior Mount Solid Antifade (Abberior GmbH, Göttingen). STED images were acquired using a Leica SP8 STED 3X (Leica Microsystems, Nanterre) equipped with a pulsed white light laser as an excitation source and the 775 nm pulsed laser as depletion light source. All images were acquired at 400 Hz through a Plan Apochromat 93×/1.3 NA glycerol objective using the LAS X software (Leica Microsystems, Nanterre). CEP164 and Arl13 were immunostained with a goat anti-mouse-IgG Star Red (Abberior GmbH, Göttingen) secondary antibody and imaged with 633 nm excitation and 775 nm depletion wavelengths. γ-tubulin was immunostained with a goat anti-rabbit-IgG Alexa Fluor 594 (Fisher Scientific, Illkirch) secondary antibody and confocally imaged with a 561 nm excitation wavelength. All STED images had a 17-nm pixel size. All images were deconvolved with Huygens Professional version 18.10 (Scientific Volume Imaging, The Netherlands, http://svi.nl), using the CMLE algorithm, with, respectively, SNR:20 and SNR:14 for the confocal and STED images with 40 iterations.

Transmission electron microscopy
For ultrastructural analysis, RPE-1 cells were fixed in 1.6% glutaraldehyde in 0.1 M phosphate buffer, rinsed in 0.1 M cacodylate buffer, post-fixed for 1 h in 1% osmium tetroxide and 1% potassium ferrocyanide in 0.1 M cacodylate buffer to enhance the staining of membranes. Cells were rinsed in distilled water, dehydrated in alcohol and finally embedded in epoxy resin. Contrasted ultrathin sections (70 nm) were analyzed using a JEOL 1400 transmission electron microscope mounted with a Morada Olympus CCD camera.

Quantifications
Results are the mean of three to five independent experiments. The error bars represent standard deviations within *n* experiments (*n*=number of distinct experiments, unless otherwise indicated). Statistical significances (*P*) were calculated using a unpaired Student's *t*-test and denoted *P<0.05; **P<0.01, ***P<0.001 and ****P<0.0001.

For cilium length measurement, fluorescence image stacks of MDCK cells obtained by laser scanning confocal microscopy (LSM780, Carl Zeiss, France) were analyzed to measure cilia lengths using a custom-built ImageJ macro program. After maximal projection of the stack, filtering by 'background subtraction', segmentation by thresholding and skeletization of the cilia, the length of the skeleton was measured to determine the length of each cilium in the image.

For RPE-1 and ARPE-19 ciliation quantification, cells were serum starved for 24 h, unless otherwise stated, fixed and processed for immunostaining and indirect immunofluorescence as described above. Cilia, preciliary membrane, distal appendage, and centriolar proteins were imaged using a 63× (1.4 NA) objective in more than six fields and, for each image, between 10 and 15 confocal *xz* sections were acquired to obtain a *z*-stack (with 450 nm step size). Images were analyzed using Image J software.

Supplemental material
Fig. S1 shows the efficiency of the different si-RNA used to deplete the expression of EFA6 isoforms and the specific role of EFA6A in ciliogenesis. Fig. S2 completes the role of EFA6A and Arf6 in PC formation in MDCK cell model. Fig. S3 shows the accumulation of GFP–EFA6A at the CEP164-labeled m-centriole during ciliogenesis. Fig. S4 shows the accumulation of Arl13B positive structures at the CEP164-labeled m-centriole in EFA6A-depleted RPE-1 cells. Fig. S5 shows that EFA6A as EFA6B interacts with Arl13B, does not act as GEF and does not rescue the inhibition of ciliogenesis induced by the depletion of Arl13B. Movie 1 is cited in Fig. S4 and shows, by 3D deconvolution confocal imaging, the accumulation of GFP–EFA6A at the m-centriole. Movie 2 is cited in Fig. 4 and shows the accumulation of Arl13B-containing vesicles at the m-centriole in EFA6A depleted RPE-1 cells by deconvolution STED 3D microscopy.

Competing interests
The authors declare no competing or financial interests.

Author contributions
Conceptualization: R.G., A.B., F.L., M.F.; Methodology: S.A., E.M., F.B.; Software: S.A., F.B.; Validation: M.P., C.L.B., R.F., S.P., S.L.-G., M.F.; Formal analysis: E.M.; Investigation: M.P., C.L.B., R.G., R.F., S.P., E.M., S.L.-G., M.F.; Resources: M.P., C.L.B., R.F.; Data curation: S.A.; Writing - original draft: A.B., F.L., M.F.; Writing - review & editing: M.F.; Supervision: S.L.-G., F.L.; M.F.; Project administration: M.F.; Funding acquisition: F.L., M.F.

Supplementary information
Supplementary information available online at
https://jcs.biologists.org/lookup/doi/10.1242/jcs.249565.supplemental

References
Badano, J. L., Mitsuma, N., Beales, P. L. and Katsanis, N. (2006). The ciliopathies: an emerging class of human genetic disorders. *Annu. Rev. Genomics Hum. Genet.* **7**, 125-148. doi:10.1146/annurev.genom.7.080505.115610

Barral, D. C., Garg, S., Casalou, C., Watts, G. F., Sandoval, J. L., Ramalho, J. S., Hsu, V. W. and Brenner, M. B. (2012). Arl13b regulates endocytic recycling traffic. *Proc. Natl. Acad. Sci. USA* **109**, 21354-21359. doi:10.1073/pnas.1218272110

Blacque, O. E., Perens, E. A., Boroevich, K. A., Inglis, P. N., Li, C., Warner, A., Khattra, J., Holt, R. A., Ou, G., Mah, A. K. et al. (2005). Functional genomics of the cilium, a sensory organelle. *Curr. Biol.* **15**, 935-941. doi:10.1016/j.cub.2005.04.059

Cantagrel, V., Silhavy, J. L., Bielas, S. L., Swistun, D., Marsh, S. E., Bertrand, J. Y., Audollent, S., Attie-Bitach, T., Holden, K. R., Dobyns, W. B. et al. (2008).

Mutations in the cilia gene ARL13B lead to the classical form of Joubert syndrome. *Am. J. Hum. Genet.* **83**, 170-179. doi:10.1016/j.ajhg.2008.06.023

Caplan, S., Naslavsky, N., Hartnell, L. M., Lodge, R., Polishchuk, R. S., Donaldson, J. G. and Bonifacino, J. S. (2002). A tubular EHD1-containing compartment involved in the recycling of major histocompatibility complex class I molecules to the plasma membrane. *EMBO J.* **21**, 2557-2567. doi:10.1093/emboj/21.11.2557

Choi, S., Ko, J., Lee, J. R., Lee, H. W., Kim, K., Chung, H. S., Kim, H. and Kim, E. (2006). ARF6 and EFA6A regulate the development and maintenance of dendritic spines. *J. Neurosci.* **26**, 4811-4819. doi:10.1523/JNEUROSCI.4182-05.2006

D'Souza-Schorey, C. and Chavrier, P. (2006). ARF proteins: roles in membrane traffic and beyond. *Nat. Rev. Mol. Cell Biol.* **7**, 347-358. doi:10.1038/nrm1910

D'Souza-Schorey, C., Li, G., Colombo, M. I. and Stahl, P. D. (1995). A regulatory role for ARF6 in receptor-mediated endocytosis. *Science* **267**, 1175-1178. doi:10.1126/science.7855600

Das, A. and Guo, W. (2011). Rabs and the exocyst in ciliogenesis, tubulogenesis and beyond. *Trends Cell Biol.* **21**, 383-386. doi:10.1016/j.tcb.2011.03.006

Decressac, S., Franco, M., Bendahhou, S., Warth, R., Knauer, S., Barhanin, J., Lazdunski, M. and Lesage, F. (2004). ARF6-dependent interaction of the TWIK1 K(+) channel with EFA6, a GDP/GTP exchange factor for ARF6. *EMBO Rep.* **5**, 1171-1175. doi:10.1038/sj.embor.7400292

Deretic, D. (2013). Crosstalk of Arf and Rab GTPases en route to cilia. *Small GTPases* **4**, 70-77. doi:10.4161/sgtp.24396

Derrien, V., Couillault, C., Franco, M., Martineau, S., Montcourrier, P., Houlgatte, R. and Chavrier, P. (2002). A conserved C-terminal domain of EFA6-family ARF6-guanine nucleotide exchange factors induces lengthening of microvilli-like membrane protrusions. *J. Cell Sci.* **115**, 2867-2879.

Donaldson, J. G. and Jackson, C. L. (2011). ARF family G proteins and their regulators: roles in membrane transport, development and disease. *Nat. Rev. Mol. Cell Biol.* **12**, 362-375. doi:10.1038/nrm3117

Eva, R., Koseki, H., Kanamarlapudi, V. and Fawcett, J. W. (2017). EFA6 regulates selective polarised transport and axon regeneration from the axon initial segment. *J. Cell Sci.* **130**, 3663-3675. doi:10.1242/jcs.207423

Franco, M., Chardin, P., Chabre, M. and Paris, S. (1995). Myristoylation of ADP-ribosylation factor 1 facilitates nucleotide exchange at physiological Mg2+ levels. *J. Biol. Chem.* **270**, 1337-1341. doi:10.1074/jbc.270.3.1337

Franco, M., Boretto, J., Robineau, S., Monier, S., Goud, B., Chardin, P. and Chavrier, P. (1998). ARNO3, a Sec7-domain guanine nucleotide exchange factor for ADP ribosylation factor 1, is involved in the control of Golgi structure and function. *Proc. Natl. Acad. Sci. USA* **95**, 9926-9931. doi:10.1073/pnas.95.17.9926

Franco, M., Peters, P. J., Boretto, J., van Donselaar, E., Neri, A., D'Souza-Schorey, C. and Chavrier, P. (1999). EFA6, a sec7 domain-containing exchange factor for ARF6, coordinates membrane recycling and actin cytoskeleton organization. *EMBO J.* **18**, 1480-1491. doi:10.1093/emboj/18.6.1480

Ghossoub, R., Molla-Herman, A., Bastin, P. and Benmerah, A. (2011). The ciliary pocket: a once-forgotten membrane domain at the base of cilia. *Biol. Cell* **103**, 131-144. doi:10.1042/BC20100128

Gong, Q., Weide, M., Huntsman, C., Xu, Z., Jan, L. Y. and Ma, D. (2007). Identification and characterization of a new class of trafficking motifs for controlling clathrin-independent internalization and recycling. *J. Biol. Chem.* **282**, 13087-13097. doi:10.1074/jbc.M700767200

Gotthardt, K., Lokaj, M., Koerner, C., Falk, N., Giessl, A. and Wittinghofer, A. (2015). A G-protein activation cascade from Arl13B to Arl3 and implications for ciliary targeting of lipidated proteins. *Elife* **4**, e11859. doi:10.7554/eLife.11859

Hattula, K., Furuhjelm, J., Tikkanen, J., Tanhuanpaa, K., Laakkonen, P. and Peranen, J. (2006). Characterization of the Rab8-specific membrane traffic route linked to protrusion formation. *J. Cell Sci.* **119**, 4866-4877. doi:10.1242/jcs.03275

Hildebrandt, F., Benzing, T. and Katsanis, N. (2011). Ciliopathies. *N. Engl. J. Med.* **364**, 1533-1543. doi:10.1056/NEJMra1010172

Hokanson, D. E. and Bretscher, A. P. (2012). EPI64 interacts with Slp1/JFC1 to coordinate Rab8a and Arf6 membrane trafficking. *Mol. Biol. Cell* **23**, 701-715. doi:10.1091/mbc.e11-06-0521

Hori, Y., Kobayashi, T., Kikko, Y., Kontani, K. and Katada, T. (2008). Domain architecture of the atypical Arf-family GTPase Arl13b involved in cilia formation. *Biochem. Biophys. Res. Commun.* **373**, 119-124. doi:10.1016/j.bbrc.2008.06.001

Ishikawa, H. and Marshall, W. F. (2011). Ciliogenesis: building the cell's antenna. *Nat. Rev. Mol. Cell Biol.* **12**, 222-234. doi:10.1038/nrm3085

Ivanova, A. A., Caspary, T., Seyfried, N. T., Duong, D. M., West, A. B., Liu, Z. and Kahn, R. A. (2017). Biochemical characterization of purified mammalian ARL13B protein indicates that it is an atypical GTPase and ARL3 guanine nucleotide exchange factor (GEF). *J. Biol. Chem.* **292**, 11091-11108. doi:10.1074/jbc.M117.784025

Klein, S., Partisani, M., Franco, M. and Luton, F. (2008). EFA6 facilitates the assembly of the tight junction by coordinating an Arf6-dependent and -independent pathway. *J. Biol. Chem.* **283**, 30129-30138. doi:10.1074/jbc.M803375200

Knodler, A., Feng, S., Zhang, J., Zhang, X., Das, A., Peranen, J. and Guo, W. (2010). Coordination of Rab8 and Rab11 in primary ciliogenesis. *Proc. Natl. Acad. Sci. USA* **107**, 6346-6351. doi:10.1073/pnas.1002401107

Larkins, C. E., Aviles, G. D., East, M. P., Kahn, R. A. and Caspary, T. (2011). Arl13b regulates ciliogenesis and the dynamic localization of Shh signaling proteins. *Mol. Biol. Cell* 22, 4694-4703. doi:10.1091/mbc.e10-12-0994

Li, Y., Tian, X., Ma, M., Jerman, S., Kong, S., Somlo, S. and Sun, Z. (2016). Deletion of ADP ribosylation factor-like GTPase 13B leads to kidney cysts. *J. Am. Soc. Nephrol.* 27, 3628-3638. doi:10.1681/ASN.2015091004

Liu, Q., Tan, G., Levenkova, N., Li, T., Pugh, E. N., Jr, Rux, J. J., Speicher, D. W. and Pierce, E. A. (2007). The proteome of the mouse photoreceptor sensory cilium complex. *Mol. Cell. Proteomics* 6, 1299-1317. doi:10.1074/mcp.M700054-MCP200

Lobo, G. P., Fulmer, D., Guo, L., Zuo, X., Dang, Y., Kim, S.-H., Su, Y., George, K., Obert, E., Fogelgren, B. et al. (2017). The exocyst is required for photoreceptor ciliogenesis and retinal development. *J. Biol. Chem.* 292, 14814-14826. doi:10.1074/jbc.M117.795674

Lu, H., Toh, M. T., Narasimhan, V., Thamilselvam, S. K., Choksi, S. P. and Roy, S. (2015a). A function for the Joubert syndrome protein Arl13b in ciliary membrane extension and ciliary length regulation. *Dev. Biol.* 397, 225-236. doi:10.1016/j.ydbio.2014.11.009

Lu, Q., Insinna, C., Ott, C., Stauffer, J., Pintado, P. A., Rahajeng, J., Baxa, U., Walia, V., Cuenca, A., Hwang, Y.-S. et al. (2015b). Early steps in primary cilium assembly require EHD1/EHD3-dependent ciliary vesicle formation. *Nat. Cell Biol.* 17, 531. doi:10.1038/ncb3155

Luton, F., Klein, S., Chauvin, J. P., Le Bivic, A., Bourgoin, S., Franco, M. and Chardin, P. (2004). EFA6, exchange factor for ARF6, regulates the actin cytoskeleton and associated tight junction in response to E-cadherin engagement. *Mol. Biol. Cell* 15, 1134-1145. doi:10.1091/mbc.e03-10-0751

Macia, E., Partisani, M., Favard, C., Mortier, E., Zimmermann, P., Carlier, M. F., Gounon, P., Luton, F. and Franco, M. (2008). The pleckstrin homology domain of the Arf6-specific exchange factor EFA6 localizes to the plasma membrane by interacting with phosphatidylinositol 4,5-bisphosphate and F-actin. *J. Biol. Chem.* 283, 19836-19844. doi:10.1074/jbc.M800781200

Macia, E., Partisani, M., Paleotti, O., Luton, F. and Franco, M. (2012). Arf6 negatively controls the rapid recycling of the beta2 adrenergic receptor. *J. Cell Sci.* 125, 4026-4035. doi:10.1242/jcs.102343

Macia, E., Partisani, M., Wang, H., Lacas-Gervais, S., Le Clainche, C., Luton, F. and Franco, M. (2019). The C-terminal domain of EFA6A interacts directly with F-actin and assembles F-actin bundles. *Sci. Rep.* 9, 19209. doi:10.1038/s41598-019-55630-9

Malicki, J. J. and Johnson, C. A. (2017). The cilium: cellular antenna and central processing unit. *Trends Cell Biol.* 27, 126-140. doi:10.1016/j.tcb.2016.08.002

Milanini, J., Fayad, R., Partisani, M., Lecine, P., Borg, J. P., Franco, M. and Luton, F. (2018). EFA6 proteins regulate lumen formation through α-actinin 1. *J. Cell Sci.* 131, jcs209361. doi:10.1242/jcs.209361

Montagnac, G., Sibarita, J. B., Loubery, S., Daviet, L., Romao, M., Raposo, G. and Chavrier, P. (2009). ARF6 Interacts with JIP4 to control a motor switch mechanism regulating endosome traffic in cytokinesis. *Curr. Biol.* 19, 184-195. doi:10.1016/j.cub.2008.12.043

Nachury, M. V., Loktev, A. V., Zhang, Q., Westlake, C. J., Peranen, J., Merdes, A., Slusarski, D. C., Scheller, R. H., Bazan, J. F., Sheffield, V. C. et al. (2007). A core complex of BBS proteins cooperates with the GTPase Rab8 to promote ciliary membrane biogenesis. *Cell* 129, 1201-1213. doi:10.1016/j.cell.2007.03.053

Peranen, J. (2011). Rab8 GTPase as a regulator of cell shape. *Cytoskeleton* 68, 527-539. doi:10.1002/cm.20529

Prigent, M., Dubois, T., Raposo, G., Derrien, V., Tenza, D., Rossé, C., Camonis, J. and Chavrier, P. (2003). ARF6 controls post-endocytic recycling through its downstream exocyst complex effector. *J. Cell Biol.* 163, 1111-1121. doi:10.1083/jcb.200305029

Quinlan, R. J., Tobin, J. L. and Beales, P. L. (2008). Modeling ciliopathies: primary cilia in development and disease. *Curr. Top. Dev. Biol.* 84, 249-310. doi:10.1016/S0070-2153(08)00605-4

Radhakrishna, H. and Donaldson, J. G. (1997). ADP-ribosylation factor 6 regulates a novel plasma membrane recycling pathway. *J. Cell Biol.* 139, 49-61. doi:10.1083/jcb.139.1.49

Rogers, K. K., Wilson, P. D., Snyder, R. W., Zhang, X., Guo, W., Burrow, C. R. and Lipschutz, J. H. (2004). The exocyst localizes to the primary cilium in MDCK cells. *Biochem. Biophys. Res. Commun.* 319, 138-143. doi:10.1016/j.bbrc.2004.04.165

Sakagami, H. (2008). The EFA6 family: guanine nucleotide exchange factors for ADP ribosylation factor 6 at neuronal synapses. *Tohoku J. Exp. Med.* 214, 191-198. doi:10.1620/tjem.214.191

Sakagami, H., Honma, T., Sukegawa, J., Owada, Y., Yanagisawa, T. and Kondo, H. (2007). Somatodendritic localization of EFA6A, a guanine nucleotide exchange factor for ADP-ribosylation factor 6, and its possible interaction with alpha-actinin in dendritic spines. *Eur. J. Neurosci.* 25, 618-628. doi:10.1111/j.1460-9568.2007.05345.x

Sanchez, I. and Dynlacht, B. D. (2016). Cilium assembly and disassembly. *Nat. Cell Biol.* 18, 711-717. doi:10.1038/ncb3370

Seixas, C., Choi, S. Y., Polgar, N., Umberger, N. L., East, M. P., Zuo, X., Moreiras, H., Ghossoub, R., Benmerah, A., Kahn, R. A. et al. (2016). Arl13b and the exocyst interact synergistically in ciliogenesis. *Mol. Biol. Cell* 27, 308-320. doi:10.1091/mbc.e15-02-0061

Sironi, C., Teesalu, T., Muggia, A., Fontana, G., Marino, F., Savaresi, S. and Talarico, D. (2009). EFA6A encodes two isoforms with distinct biological activities in neuronal cells. *J. Cell Sci.* 122, 2108-2118. doi:10.1242/jcs.042325

Sorokin, S. (1962). Centrioles and the formation of rudimentary cilia by fibroblasts and smooth muscle cells. *J. Cell Biol.* 15, 363-377. doi:10.1083/jcb.15.2.363

Sun, Z., Amsterdam, A., Pazour, G. J., Cole, D. G., Miller, M. S. and Hopkins, N. (2004). A genetic screen in zebrafish identifies cilia genes as a principal cause of cystic kidney. *Development* 131, 4085-4093. doi:10.1242/dev.01240

Thomas, S., Boutaud, L., Reilly, M. L. and Benmerah, A. (2019). Cilia in hereditary cerebral anomalies. *Biol. Cell* 111, 217-231. doi:10.1111/boc.201900012

Tobin, J. L. and Beales, P. L. (2009). The nonmotile ciliopathies. *Genet. Med.* 11, 386-402. doi:10.1097/GIM.0b013e3181a02882

Tsang, W. Y. and Dynlacht, B. D. (2013). CP110 and its network of partners coordinately regulate cilia assembly. *Cilia* 2, 9. doi:10.1186/2046-2530-2-9

Wei, Q., Ling, K. and Hu, J. (2015). The essential roles of transition fibers in the context of cilia. *Curr. Opin. Cell Biol.* 35, 98-105. doi:10.1016/j.ceb.2015.04.015

Westlake, C. J., Baye, L. M., Nachury, M. V., Wright, K. J., Ervin, K. E., Phu, L., Chalouni, C., Beck, J. S., Kirkpatrick, D. S., Slusarski, D. C. et al. (2011). Primary cilia membrane assembly is initiated by Rab11 and transport protein particle II (TRAPPII) complex-dependent trafficking of Rabin8 to the centrosome. *Proc. Natl. Acad. Sci. USA* 108, 2759-2764. doi:10.1073/pnas.1018823108

Wu, C. T., Chen, H. Y. and Tang, T. K. (2018). Myosin-Va is required for preciliary vesicle transportation to the mother centriole during ciliogenesis. *Nat. Cell Biol.* 20, 175-185. doi:10.1038/s41556-017-0018-7

Yoshimura, S., Egerer, J., Fuchs, E., Haas, A. K. and Barr, F. A. (2007). Functional dissection of Rab GTPases involved in primary cilium formation. *J. Cell Biol.* 178, 363-369. doi:10.1083/jcb.200703047

Zangari, J., Partisani, M., Bertucci, F., Milanini, J., Bidaut, G., Berruyer-Pouyet, C., Finetti, P., Long, E., Brau, F., Cabaud, O. et al. (2014). EFA6B antagonizes breast cancer. *Cancer Res.* 74, 5493-5506. doi:10.1158/0008-5472.CAN-14-0298

Zuo, X., Guo, W. and Lipschutz, J. H. (2009). The exocyst protein Sec10 is necessary for primary ciliogenesis and cystogenesis in vitro. *Mol. Biol. Cell* 20, 2522-2529. doi:10.1091/mbc.e08-07-0772